Supersymmetric QCD and CP-violation effects in $t\bar{t}Z^0$ production at the LHC

Liu Ning, Guo Lei, Ma Wen-Gan, Zhang Ren-You, and Han Liang

Department of Modern Physics, University of Science and Technology of China (USTC), Hefei, Anhui 230026, P.R.China

Abstract

We investigate the NLO QCD and the CP-violation effects in $t\bar{t}Z^0$ production at the Large Hadron Collider(LHC) in the minimal supersymmetric standard model(MSSM). Our calculation shows that the total NLO QCD correction in the framework of the CP-conserving MSSM significantly improves the scale uncertainty at the leading order, and the contribution from the pure supersymmetric QCD (pSQCD) correction can exceed -8% with the restrictions of 90 $GeV < p_T^t < 120$ GeV and 120 $GeV < p_T^Z < 150$ GeV, where p_T^t and p_T^Z are the transverse momenta of the top-quark and Z^0 gauge boson, respectively. Our numerical results demonstrate that the pure supersymmetric QCD correction generally suppresses the total SM-like QCD correction in the CP-conserving MSSM, and tends to be a constant when either $\tilde{t}_1$ or $\tilde{g}$ is heavy enough. We find also that the CP-odd asymmetry $\mathcal{A}_\Phi$ can reach 2.17×10^{-3}, if the CP-phase angle really exists in the coupling of gluino-stop-top.

PACS: 12.60.Jv, 14.70.Hp, 14.65.Ha, 12.38.Bx

I. Introduction

Although the standard model(SM)[1, 2] has achieved great success in describing all the available experimental data, it suffers from some conceptional difficulties. That has triggered an intense activity in developing extension models. The supersymmetric (SUSY) extensions[3, 4, 5, 6, 7]) rank among the most promising and well-explored scenarios for new physics at the TeV scale. Apart from predicting a light Higgs boson and describing the low energy experimental data very well, the SUSY models are able to solve various theoretical problems, e.g., the SUSY models may provide an elegant way to construct the huge hierarchy between the electroweak symmetry breaking(EWSB) scale and the grand unification scale. At present the minimal supersymmetric standard model(MSSM)[8] is regarded as the simplest and the most attractive one in the SUSY models.

The direct evidence for the top-quark was presented in 1995 by the CDF and D0 collaborations of the Fermilab Tevatron[9, 10]. This is considered to be a remarkable success of the SM. From that time on the top physics program has been turned to precise investigation for its properties. Since the top quark is the heaviest particle in the SM detected until now, it plays a special role in the mechanism of the EWSB, and the new physics connected to the EWSB may be found firstly through precise study of top-quark observables. The high accumulated top-quark events at the CERN LHC will open a new, rich field of top-quark phenomenology. Deviations of experimental measurements from the SM predictions, would indicate new non-standard top production or decay mechanisms. Therefore, the precise study of the top properties is one of the urgent priorities of the high energy experimental program.

Beside the SUSY particle direct production, virtual effects of SUSY particles may induce deviations on observables from the SM predictions. If SUSY particles are really detected at the LHC, the comparison of precisely measured top-quark observables with the theoretical predictions including SUSY loop effects may yield additional information about the underlying model. Therefore, probing precisely the properties of the top-quark is an important goal at the LHC. In order to study precisely the top-quark physics within the SM and beyond at the LHC, it is necessary to give the theoretical predictions for top-quark observables including

higher-order corrections. In Ref.[11] S. Berge et al., provide the predictions including the NLO SUSY QCD effects in the MSSM for the total production rate and kinematic distributions of polarized and unpolarized top-quark pair production at the Tevatron and the LHC.

Probing the couplings between the top quark and gauge bosons is another way to discover new physics. Until now there have been many works which devote to the observables related to the top-quark gauge couplings in the SM and beyond. The theoretical study of the effects of the top-quark and Z^0 gauge boson coupling at colliders was widely carried out. The calculations for the process $e^+e^- \to t\bar{t}Z^0$ at the leading-order(LO) and including next-to-leading order(NLO) QCD, electroweak corrections in the context of the SM were presented in Refs. [12, 13], respectively, while CP-violating effects in $e^+e^- \to t\bar{t}Z^0$ process were studied in the framework of the two Higgs doublets model(THDM)[14] and with model independent effective Lagrangian[15]. The $\gamma\gamma \to t\bar{t}Z^0$ production channel has an outstanding advantage over $e^+e^- \to t\bar{t}Z^0$ process in measuring $t\bar{t}Z^0$ coupling at the ILC, due to its relatively larger production rate[16, 17]. The NLO SUSY QCD corrections to the $\gamma\gamma \to t\bar{t}Z^0$ process at linear colliders, and the NLO SM QCD corrections to the $t\bar{t}Z^0$ production at the LHC are studied in Refs.[18] and [19], respectively.

In this work, we calculate the production of the top-quark pair associated with a Z^0 boson at the CERN LHC in both the leading-order(LO) and NLO QCD approximations in the framework of the MSSM with CP-conservation or CP-violation, and investigate the possible CP-violating effects contributed by the CP-phase in the couplings of gluino-stop-top predicted by the CP-violating MSSM. The paper is organized as follows: The description of the related theory about the CP-conserving and CP-violating MSSM is presented in section 2. In section 3 we outline the technical details of the related LO and NLO QCD calculations. In Sec.4 we give some numerical results and discussions about the NLO SUSY QCD corrections and the possible CP-odd effect. Finally, a short summary is given.

II. Related theory of the CP-violating MSSM

In the MSSM, each quark has two scalar partners called squarks, $\tilde{q}_L$ and $\tilde{q}_R$(or $\tilde{q}_1$ and $\tilde{q}_2$). The mass term of scalar quarks can be written as[20]

$$-\mathcal{L}_{\tilde{q}}^{mass} = \left(\begin{array}{cc} \tilde{q}_L^\dagger & \tilde{q}_R^\dagger \end{array} \right) \mathcal{M}_{\tilde{q}}^2 \left(\begin{array}{c} \tilde{q}_L \\ \tilde{q}_R \end{array} \right), \tag{2.1}$$

where $\mathcal{M}_{\tilde{q}}^2$ is the mass squared matrix of $\tilde{q}_L$ and $\tilde{q}_R$, expressed as

$$\mathcal{M}_{\tilde{q}}^2 = \left(\begin{array}{cc} m_{\tilde{q}_L}^2 & a_q m_q \\ a_q^* m_q & m_{\tilde{q}_R}^2 \end{array} \right). \tag{2.2}$$

The diagonal and nondiagonal elements of this mass squared matrix are

$$\begin{aligned} m_{\tilde{q}_L}^2 &= \tilde{M}_Q^2 + m_q^2 + m_Z^2 (I_q^3 - Q_q s_W^2) \cos 2\beta, \\ m_{\tilde{q}_R}^2 &= \tilde{M}_{U,D}^2 + m_q^2 + Q_q m_Z^2 s_W^2 \cos 2\beta, \\ a_q m_q &= m_q \left(A_q - \mu r_{U,D} \right), \end{aligned} \tag{2.3}$$

where m_q, Q_q and I_q^3 are the mass, electric charge and the third component of the weak isospin of the quark q, μ is the Higgsino mass parameter, A_q ($q = u, d, c, s, t, b$) are the supersymmetry soft-breaking trilinear coupling constants, $\tilde{M}_Q^2$, $\tilde{M}_U^2$ and $\tilde{M}_D^2$ are the supersymmetry soft-breaking mass parameters of the left- and right-handed scalar quarks, and $r_U = 1/r_D = \cot\beta$ are for the up- and down-type squarks, respectively. The mass squared matrix $\mathcal{M}_{\tilde{q}}^2$ can be diagonalized by introducing a unitary matrix $\mathcal{R}^{\tilde{q}}$. The mass eigenstates $\tilde{q}_1$, $\tilde{q}_2$ are defined as

$$\left(\begin{array}{c} \tilde{q}_1 \\ \tilde{q}_2 \end{array} \right) = \mathcal{R}^{\tilde{q}} \left(\begin{array}{c} \tilde{q}_L \\ \tilde{q}_R \end{array} \right). \tag{2.4}$$

Then the mass term of scalar quarks can be expressed as

$$-\mathcal{L}_{\tilde{q}}^{mass} = \left(\begin{array}{cc} \tilde{q}_1^\dagger & \tilde{q}_2^\dagger \end{array} \right) \mathcal{M}_D^{\tilde{q}\,2} \left(\begin{array}{c} \tilde{q}_1 \\ \tilde{q}_2 \end{array} \right), \tag{2.5}$$

where

$$\mathcal{M}_D^{\tilde{q}\,2} = \mathcal{R}^{\tilde{q}} \mathcal{M}_{\tilde{q}}^2 \mathcal{R}^{\tilde{q}\,\dagger} = \left(\begin{array}{cc} m_{\tilde{q}_1}^2 & 0 \\ 0 & m_{\tilde{q}_2}^2 \end{array} \right). \tag{2.6}$$

It is well known that the unitary matrix $\mathcal{R}^{\tilde{q}}$ can be parameterized as

$$\mathcal{R}^{\tilde{q}} = \left(\begin{array}{cc} \cos\theta_q e^{-i\phi_q} & \sin\theta_q e^{i\phi_q} \\ -\sin\theta_q e^{-i\phi_q} & \cos\theta_q e^{i\phi_q} \end{array} \right), \tag{2.7}$$

where θ_q is called as the mixing angle between the left- and right-handed squarks, and $2\phi_q$ is the phase angle of a_q defined as $a_q = |a_q|e^{2i\phi_q}$. The masses of the squark mass eigenstates and the mixing angles acquire the forms as

$$\begin{aligned}(m^2_{\tilde{q}_1}, m^2_{\tilde{q}_2}) &= \frac{1}{2}\Big\{(m^2_{\tilde{q}_L} + m^2_{\tilde{q}_R}) \mp \left[(m^2_{\tilde{q}_L} - m^2_{\tilde{q}_R})^2 + 4|a_q|^2 m_q^2\right]^{1/2}\Big\}, \\ & \tan 2\theta_q = \frac{2m_q|a_q|}{m^2_{\tilde{q}_L} - m^2_{\tilde{q}_R}}. \end{aligned} \tag{2.8}$$

Because of the large masses of the third generation quarks, the mixing effects of the third generation squarks are more significant than the first two generations. If we take the stop masses($m_{\tilde{t}_1}$, $m_{\tilde{t}_2}$) and the stop mixing angle(θ_t) as the input parameters for the stop sector, the values of $m_{\tilde{t}_L}$, $m_{\tilde{t}_R}$ and $|a_t|$ can be obtained by adopting Eq.(2.9).

$$\begin{aligned} m^2_{\tilde{q}_L} &= \cos^2\theta_q m^2_{\tilde{q}_1} + \sin^2\theta_q m^2_{\tilde{q}_2}, \\ m^2_{\tilde{q}_R} &= \sin^2\theta_q m^2_{\tilde{q}_1} + \cos^2\theta_q m^2_{\tilde{q}_2}, \\ m_q|a_q| &= \sin\theta_q\cos\theta_q\left(m^2_{\tilde{q}_1} - m^2_{\tilde{q}_2}\right). \end{aligned} \tag{2.9}$$

In the CP-violating MSSM, the SUSY soft-breaking trilinear coupling A_q and the Higgsino mass parameter μ can be complex. That makes a_q having complex value. By using the parameterization of the unitary matrix $\mathcal{R}^{\tilde{q}}$ (Eq.(2.7)), we obtain the squark current eigenstates ($\tilde{q}_L$, $\tilde{q}_R$) in terms of the mass eigenstates ($\tilde{q}_1$, $\tilde{q}_2$) as

$$\tilde{q}_L = (\tilde{q}_1\cos\theta_q - \tilde{q}_2\sin\theta_q)e^{i\phi_q}, \quad \tilde{q}_R = (\tilde{q}_1\sin\theta_q + \tilde{q}_2\cos\theta_q)e^{-i\phi_q}. \tag{2.10}$$

Normally the CP-violating effects in the MSSM from the gluino-squark-quark interactions are much more important than from the chargino and neutralino sectors due to the strong interaction. We consider only the CP-violating effects induced by the $\tilde{g} - \tilde{t}_{1,2} - t$ strong interactions. The Lagrangian for the gluino-stop-top couplings is given by

$$\begin{aligned}\mathcal{L}_{\tilde{g}-\tilde{t}-t} &= \sqrt{2}g_s\sum_{a=1}^{8}\bar{t}T^a\Big(\epsilon\tilde{t}_R P_L - \epsilon^*\tilde{t}_L P_R\Big)\tilde{g}^a + h.c. \\ &= \sqrt{2}g_s\sum_{a=1}^{8}\sum_{\alpha,\beta=1}^{3}\bar{t}_\alpha T^a_{\alpha\beta}\Big(\epsilon\tilde{t}_{R\beta}P_L - \epsilon^*\tilde{t}_{L\beta}P_R\Big)\tilde{g}^a + h.c., \end{aligned} \tag{2.11}$$

where g_s is the strong coupling constant, $T^a = (T^a_{\alpha\beta})$ $(a = 1, ..., 8)$ are the $SU(3)$ generators, a, α, β are the color indices of gluino, top and stop separately, $P_{L,R} = (1 \mp \gamma^5)/2$ and $\epsilon = e^{-i\phi_{SU(3)}}$. Here $2\phi_{SU(3)}$ is the phase angle of $M_{SU(3)}$, the supersymmetry soft-breaking $SU(3)$ gaugino (gluino) mass parameter, which is defined as

$$M_{SU(3)} = |M_{SU(3)}| e^{2i\phi_{SU(3)}}. \tag{2.12}$$

By inserting Eq.(2.10) into Eq.(2.11), the mixing angle θ_t and phase angle ϕ_t may enter into the couplings, and the Lagrangian is expressed in terms of the stop mass eigenstates $(\tilde{t}_{1,2})$ instead of the current eigenstates $(\tilde{t}_{L,R})$ as

$$\begin{aligned} \mathcal{L}_{\tilde{g}-\tilde{t}-t} &= \sqrt{2} g_s \sum_{a=1}^{8} \bar{t} T^a \Big[\Big(\tilde{t}_1 \sin\theta_t + \tilde{t}_2 \cos\theta_t \Big) e^{-i\left(\phi_t + \phi_{SU(3)}\right)} P_L \\ &\qquad - \Big(\tilde{t}_1 \cos\theta_t - \tilde{t}_2 \sin\theta_t \Big) e^{i\left(\phi_t + \phi_{SU(3)}\right)} P_R \Big] \tilde{g}^a + h.c. \ . \end{aligned} \tag{2.13}$$

As shown in this Lagrangian, only the combination of the phase angles ϕ_t and $\phi_{SU(3)}$ enters into the gluino-stop-top couplings. Therefore, we redefine this combination as ϕ_t,

$$\phi_t + \phi_{SU(3)} \to \phi_t, \tag{2.14}$$

and obtain the conventional expression of the gluino-stop-top interaction Lagrangian as

$$\begin{aligned} \mathcal{L}_{\tilde{g}-\tilde{t}-t} &= \sqrt{2} g_s \sum_{a=1}^{8} \bar{t} T^a \Big[\Big(\tilde{t}_1 \sin\theta_t + \tilde{t}_2 \cos\theta_t \Big) e^{-i\phi_t} P_L \\ &\qquad - \Big(\tilde{t}_1 \cos\theta_t - \tilde{t}_2 \sin\theta_t \Big) e^{i\phi_t} P_R \Big] \tilde{g}^a + h.c. \\ &= -i \sum_{i=1}^{2} \sum_{a=1}^{8} \bar{t} \Big(V^L_{\tilde{g}\tilde{t}_i t} P_L + V^R_{\tilde{g}\tilde{t}_i t} P_R \Big) \tilde{g}^a \tilde{t}_i + h.c., \end{aligned} \tag{2.15}$$

where $V^L_{\tilde{g}\tilde{t}_1 t} = i\sqrt{2} g_s T^a \sin\theta_t e^{-i\phi_t}$, $V^L_{\tilde{g}\tilde{t}_2 t} = i\sqrt{2} g_s T^a \cos\theta_t e^{-i\phi_t}$, $V^R_{\tilde{g}\tilde{t}_1 t} = -i\sqrt{2} g_s T^a \cos\theta_t e^{i\phi_t}$ and $V^R_{\tilde{g}\tilde{t}_2 t} = i\sqrt{2} g_s T^a \sin\theta_t e^{i\phi_t}$. There are similar expressions for other $\tilde{g} - \tilde{q}_i - q (q = u, d, c, s, b)$ couplings involving CP-phase angles. Because in this work we consider only the CP-phase effects from the $\tilde{g} - \tilde{t}_{1,2} - t$ couplings, we take $\phi_t \neq 0$ and $\phi_q = 0$ for $q = u, d, c, s, b$.

In order to describe the CP-violating effects on the process, we take a definition of a CP-odd observable for the LHC, which is constructed to describe the distribution asymmetry of

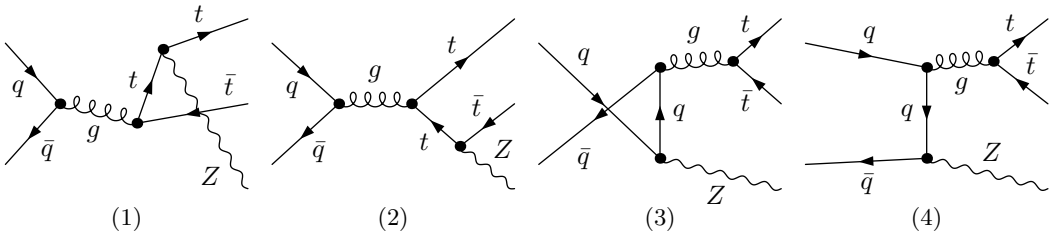

Figure 1: The LO Feynman diagrams for the $q\bar{q} \to t\bar{t}Z^0$ $(q = u, d, s, c)$ partonic process.

the azimuthal angle Φ between $\hat{p}_{\bar{t}}^T$ and $\hat{p}_t^T$ in the range of $-180^\circ \leq \Phi \leq 180^\circ$, i.e.,

$$\Phi \equiv \text{sgn}\left[(\vec{p}_t - \vec{p}_{\bar{t}}) \cdot \hat{z}\right] \ \text{sgn}\left[(\vec{p}_t \times \vec{p}_{\bar{t}}) \cdot \hat{z}\right] \cos^{-1}(\hat{p}_t^T \cdot \hat{p}_{\bar{t}}^T), \tag{2.16}$$

where Φ in Eq.(2.16) comes from the modified definition of Eq.(14) in Ref.[21], and $\hat{z}$ is a unit vector of the z-axis direction along one of the incoming proton. The CP-asymmetry of angle Φ is defined as

$$\mathcal{A}_\Phi \equiv \frac{\Delta\sigma_\Phi}{\sigma_T} = \frac{\sigma(180^\circ > \Phi > 0^\circ) - \sigma(0^\circ > \Phi > -180^\circ)}{\sigma(180^\circ > \Phi > 0^\circ) + \sigma(0^\circ > \Phi > -180^\circ)}. \tag{2.17}$$

The significance is defined as

$$S = \frac{|\Delta\sigma_\Phi|\mathcal{L}}{\sqrt{\sigma_T \mathcal{L}}}. \tag{2.18}$$

Then the CP-asymmetry effect may become observable at the $S\sigma$ significance, if the integrated luminosity has a value larger than

$$\mathcal{L} = S^2 \frac{\sigma_T}{|\Delta\sigma_\Phi|^2} = \frac{S^2}{|\mathcal{A}_\Phi|^2 \sigma_T}. \tag{2.19}$$

III. Calculations

III..1 The LO cross sections for the partonic processes

The contributions to the hadronic process of top-pair production associated with a Z^0 boson at the LO, are from the partonic processes $q\bar{q} \to t\bar{t}Z^0$ $(q = u, d, c, s)$ and $gg \to t\bar{t}Z^0$ channels. We use the 't Hooft-Feynman gauge in the following LO and NLO calculations. The LO Feynman diagrams for the subprocesses $q(p_1)\bar{q}(p_2) \to t(p_3)\bar{t}(p_4)Z^0(p_5)$, $(q = u, d, c, s)$ and $g(p_1)g(p_2) \to t(p_3)\bar{t}(p_4)Z^0(p_5)$ in the MSSM are depicted in Fig.1 and Fig.2, respectively.

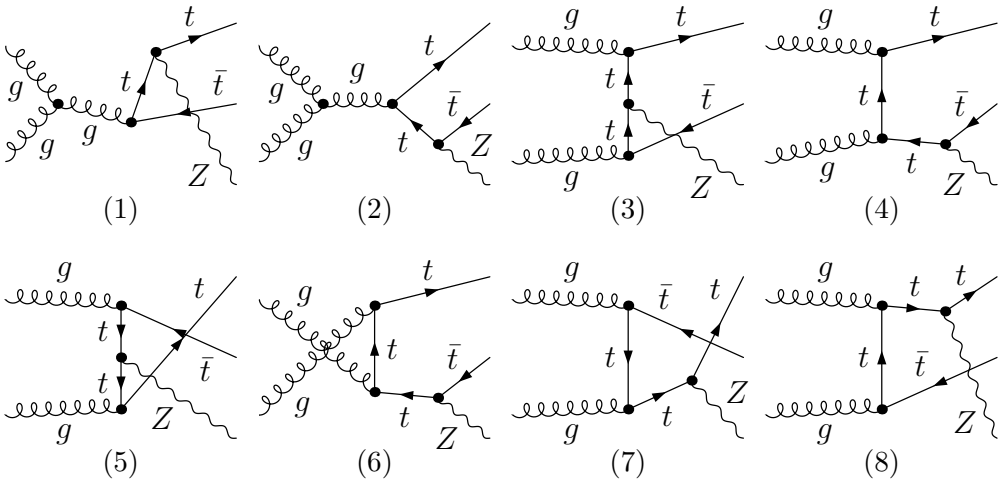

Figure 2: The LO Feynman diagrams for the $gg \to t\bar{t}Z^0$ partonic process.

The LO Feynman diagrams for all these subprocesses in the MSSM are the same as their corresponding ones in the SM. The explicit expressions of the LO cross section for the partonic processes can be written in the form as:

$$\hat{\sigma}^{ij}_{LO} = \frac{1}{4|\vec{p}_1|\sqrt{\hat{s}}} \int \mathrm{d}\Gamma_3 \overline{\sum} |\mathcal{M}^{ij}_{LO}|^2 \tag{3.1}$$

where $ij = q\bar{q}, gg(q = u, d, c, s)$, the summation is taken over the spins and colors of initial and final states, $\vec{p}_1$ is the c.m.s. momentum of one initial parton, and the bar over the summation recalls averaging over the spins and colors of initial partons. $\mathrm{d}\Gamma_3$ is the three-body phase space element expressed as

$$\mathrm{d}\Gamma_3 = (2\pi)^4 \delta^4(p_1 + p_2 - \sum_{i=3}^{5} p_i) \prod_{i=3}^{5} \frac{d^3\vec{p}_i}{(2\pi)^3 2E_i}. \tag{3.2}$$

In the LO calculation for the parent process $pp \to t\bar{t}Z^0 + X$ we involve the contributions from partonic processes $gg \to t\bar{t}Z^0$ and $q\bar{q} \to t\bar{t}Z^0$ $(q = u, d, c, s)$. Our numerical calculation shows the contribution to the LO integrated cross section from the partonic processes $s\bar{s}, c\bar{c} \to t\bar{t}Z^0$ is less than 3% at the LHC. Therefore, we consider only the NLO QCD corrections to the processes $pp \to u\bar{u}, d\bar{d}, gg \to t\bar{t}Z^0 + X$ in the following NLO calculation.

III..2 NLO QCD corrections to the partonic processes

The NLO QCD correction in the MSSM(NLO SQCD) to each of the partonic subprocess $q\bar{q} \to t\bar{t}Z^0$ $(q = u, d)$ and $gg \to t\bar{t}Z^0$ consists of two independent parts. One is the so-called SM-like

component, another is the pure SUSY QCD (pSQCD) component arising from the contributions of the virtual gluino one-loop diagrams. We adopt the dimensional regularization scheme in $D = 4 - 2\epsilon$ dimensions to isolate the ultraviolet (UV) and infrared (IR) singularities. Then the total NLO SQCD corrections to the partonic subprocess $q\bar{q} \to t\bar{t}Z^0$ $(q = u, d)$ and $gg \to t\bar{t}Z^0$, can be written as:

$$\Delta\hat{\sigma}^{ij}_{SNLO} = \Delta\hat{\sigma}^{ij}_{SM-like} + \Delta\hat{\sigma}^{ij}_{pSQCD}, \quad (ij = u\bar{u}, d\bar{d}, gg). \tag{3.3}$$

In the MSSM, the so-called SM-like NLO QCD correction component is exactly equal to the NLO QCD correction in the SM, and we shall compare our results for the SM-like correction with those in Ref.[19]. The pSQCD correction component is UV and IR finite after renormalzation. The NLO SQCD correction includes the following contributions:

- ▶ the virtual corrections to the partonic process $q\bar{q}(gg) \to t\bar{t}Z^0$.
- ▶ the real gluon emission partonic process $q\bar{q}(gg) \to t\bar{t}Z^0g$.
- ▶ the real light-(anti)quark emission partonic process $q(\bar{q})g \to t\bar{t}Z^0q(\bar{q})$.
- ▶ the collinear counterterms of the PDF.

(1) Virtual corrections in the MSSM

In the MSSM, the virtual QCD $\mathcal{O}(\alpha_s)$ corrections come from the one-loop diagrams including self-energy, vertex, box and pentagon diagrams. In Figs.3-6, we illustrate all the pentagon graphs for the partonic processes $q\bar{q} \to t\bar{t}Z^0$ and $gg \to t\bar{t}Z^0$, separately. We take the definitions of the scalar and tensor two-, three-, four- and five-point integral functions presented in Ref.[23]. We use Passarino-Veltman method[24] to reduce the N-point($N \leq 5$) tensor functions to scalar integrals, and manipulate the γ_5 matrix in D-dimensions by employing a naive scheme as presented in Ref.[25], which keeps an anticommuting γ_5 in all dimensions. The one-loop Feynman diagrams and the corresponding amplitudes are created by using FeynArts3.2 package[26], and the scalar integrals are evaluate mainly by adopting the LoopTools-2.1 package[27, 28]. In order to cancel the UV divergences from both the SM-like and pSQCD one-loop diagrams, we should introduce some suitable counterterms.

$$m_t \quad \to \quad m_t + \delta m_t = m_t + \delta m_t^{SM-like} + \delta m_t^{pSQCD},$$

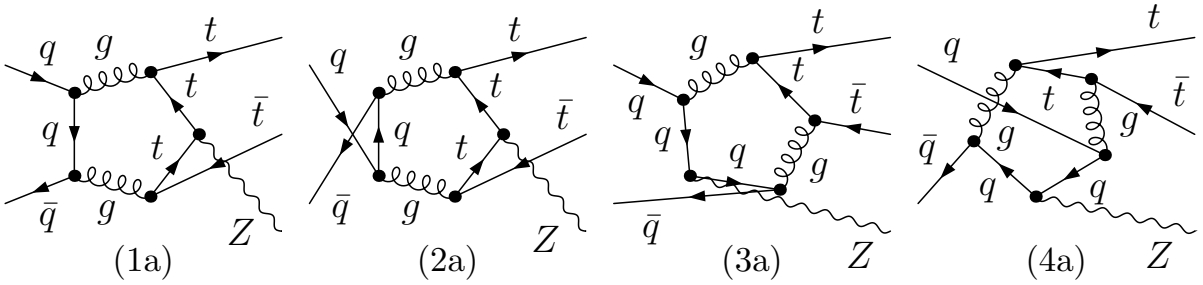

Figure 3: The SM-like pentagon Feynman diagrams for the $q\bar{q} \to t\bar{t}Z^0$ partonic process.

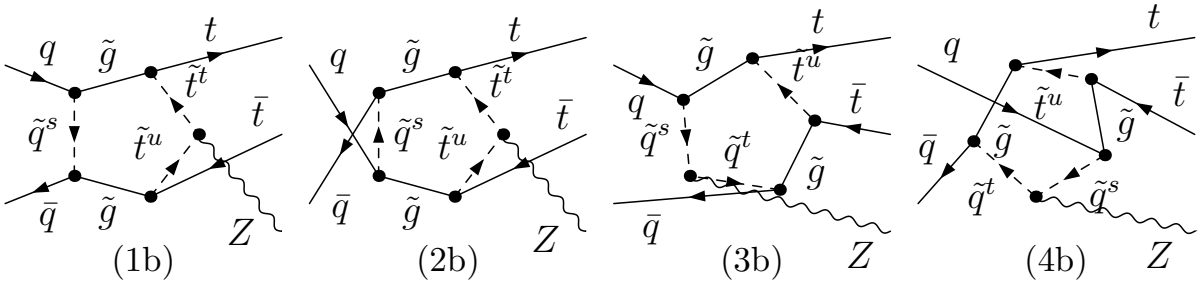

Figure 4: The pSQCD pentagon Feynman diagrams for the $q\bar{q} \to t\bar{t}Z^0$ partonic process with the upper indices in $\tilde{t}^{u,t}$ and $\tilde{q}^{s,t}$ running from 1 to 2 respectively.

$$
\begin{aligned}
g_s &\to g_s + \delta g_s = g_s + \delta g_s^{SM-like} + \delta g_s^{pSQCD}, \\
t_L &\to (1 + \frac{1}{2}\delta Z_L^t) t_L = \left[1 + \frac{1}{2}(\delta Z_L^{t,SM-like} + \delta Z_L^{t,pSQCD})\right] t_L, \\
t_R &\to (1 + \frac{1}{2}\delta Z_R^t) t_R = \left[1 + \frac{1}{2}(\delta Z_R^{t,SM-like} + \delta Z_R^{t,pSQCD})\right] t_R, \\
G_\mu^a &\to (1 + \frac{1}{2}\delta Z_g) G_\mu = \left[1 + \frac{1}{2}\left(\delta Z_g^{SM-like} + \delta Z_g^{pSQCD}\right)\right] G_\mu^a,
\end{aligned} \tag{3.4}
$$

where $t_{L,R}$ and G_μ are the wave functions of top-quark and gluon, respectively.

The counterterms of top-quark, gluon fields and top-quark mass are fixed by using on-mass-shell renormalization conditions [23]. For the renomalization of the QCD strong coupling constant g_s, we use the $\overline{MS}$ scheme except that the divergences associated with top quark and the colored SUSY particle loops are subtracted at zero momentum[22]. The counterterm of the strong coupling constant includes the SM-like and pSQCD terms, which can be expressed as follows,

$$
\frac{\delta g_s^{SM-like}}{g_s} = -\frac{\alpha_s(\mu_r)}{4\pi}\left[\frac{\beta_0^{SM-like}}{2}\frac{1}{\bar{\epsilon}} + \frac{1}{3}\ln\frac{m_t^2}{\mu_r^2}\right], \tag{3.5}
$$

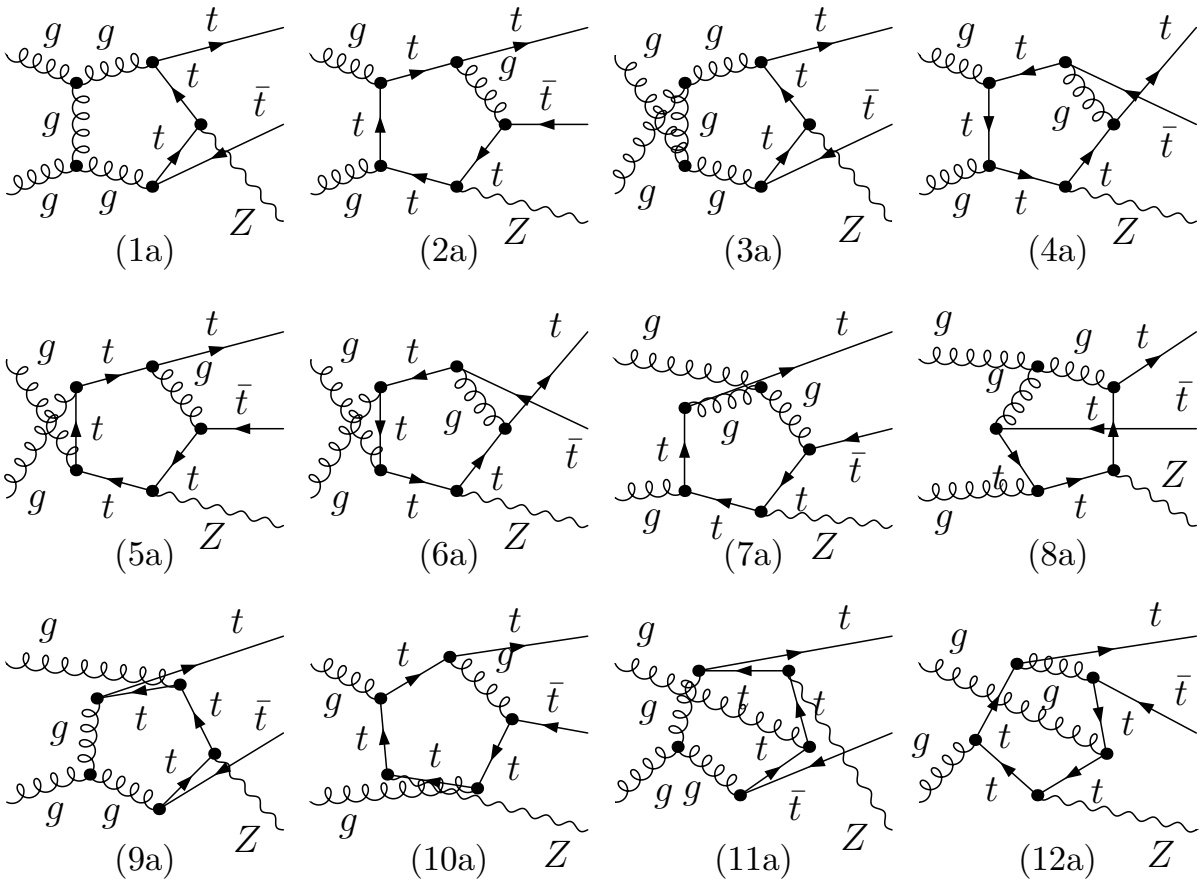

Figure 5: The SM-like pentagon Feynman diagrams for the $gg \to t\bar{t}Z^0$ partonic process. The diagrams obtained by exchanging initial gluons are not depicted.

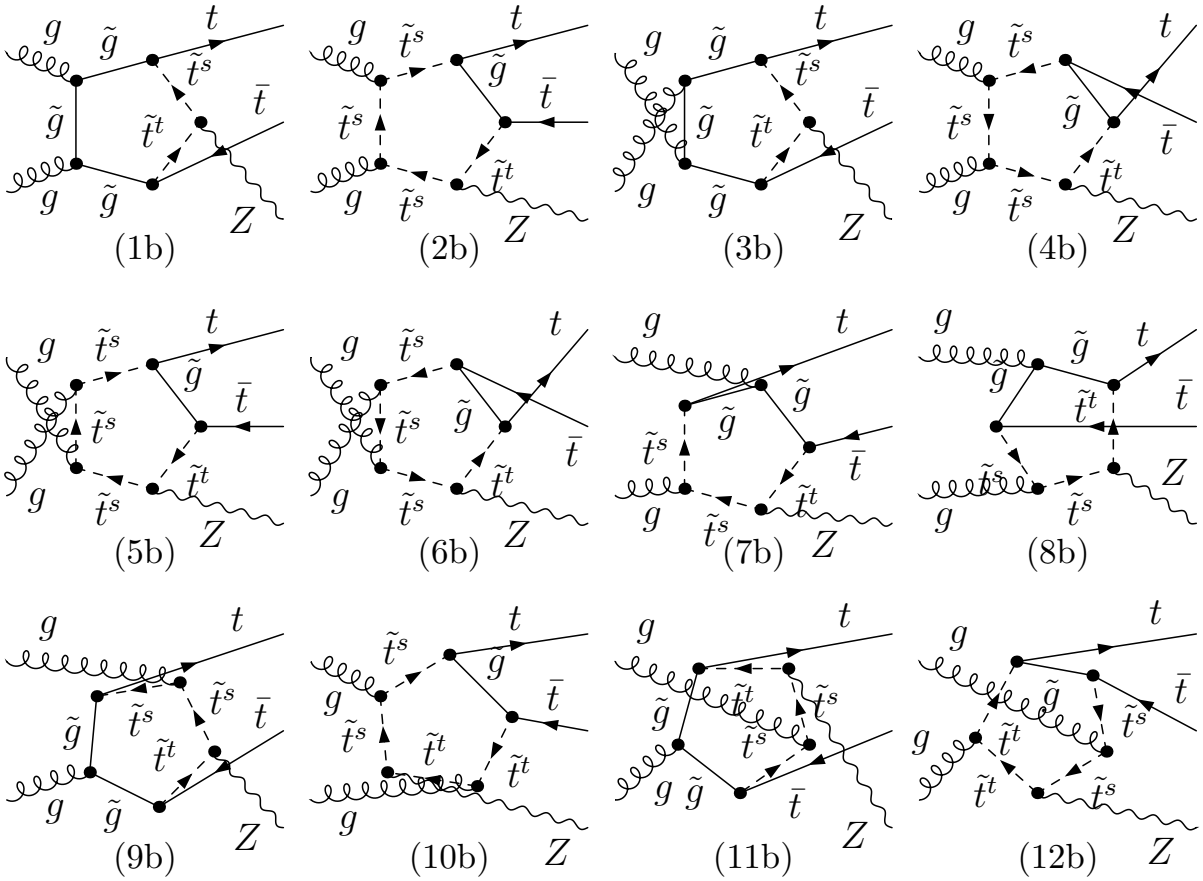

Figure 6: The pSQCD pentagon Feynman diagrams for the $gg \to t\bar{t}Z^0$ partonic process. The upper indices in $\tilde{t}^{s,t}$ run from 1 to 2 respectively. The diagrams obtained by exchanging initial gluons are not shown.

$$\frac{\delta g_s^{pSQCD}}{g_s} = -\frac{\alpha_s(\mu_r)}{4\pi}\left[\frac{\beta_1^{pSQCD}}{2\bar{\epsilon}} + \frac{N_c}{3}\ln\frac{m_{\tilde{g}}^2}{\mu_r^2} + \sum_{U=u,c,t}^{i=1,2}\frac{1}{12}\ln\frac{m_{\tilde{U}_i}^2}{\mu_r^2} + \sum_{D=d,s,b}^{j=1,2}\frac{1}{12}\ln\frac{m_{\tilde{D}_j}^2}{\mu_r^2}\right], \tag{3.6}$$

where

$$\beta_0^{(SM-like)} = \frac{11}{3}N_c - \frac{2}{3}n_{lf} - \frac{2}{3}, \quad \beta_1^{(pSQCD)} = -\frac{2}{3}N_c - \frac{1}{3}(n_{lf}+1), \tag{3.7}$$

with $N_c = 3$, $n_{lf} = 5$ light flavors and $\frac{1}{\bar{\epsilon}} = \frac{1}{\epsilon_{UV}} + \ln(4\pi) - \gamma_E$. With the introduction of the CP-violating phase ϕ_t in the MSSM, the renormalized one-particle irreducible two-point functions for top-quark and gluon containing the contributions from pSQCD are defined as follows [23, 30]

$$\hat{\Gamma}^{(t)}_{pSQCD}(p) = i\left[\not{p}P_L\hat{\Sigma}^{(t)L}_{pSQCD}(p^2) + \not{p}P_R\hat{\Sigma}^{(t)R}_{pSQCD}(p^2) + P_L\hat{\Sigma}^{(t)S}_{pSQCD}(p^2) + P_R\hat{\Sigma}^{(t)S\ \ddagger}_{pSQCD}(p^2)\right],$$

$$\hat{\Gamma}^{(g)ab}_{pSQCD}(p) = -i\left(g^{\mu\nu} - \frac{p^\mu p^\nu}{p^2}\right)\delta^{ab}\hat{\Sigma}^{(g)T}_{pSQCD}(p^2) - i\frac{p^\mu p^\nu}{p^2}\delta^{ab}\hat{\Sigma}^{(g)L}_{pSQCD}(p^2). \tag{3.8}$$

It should be mentioned here that in the first equation of Eqs.(3.8) the upper conjugation symbol ‡ acts only on the CP-violating phase. The SM-like components for the top quark, gluon self-energies, wave function and top mass counterterms, can be found in many references, such as Ref.[23]. Here we present only the related pSQCD component expressions for unrenormalized top quark, gluon self-energies and counterterms.

$$\Sigma^{(t)L}_{pSQCD}(p^2) = -\frac{C_F}{8\pi^2}g_s^2\left(\cos^2\theta_{\tilde{t}}\ B_1[p^2, m_{\tilde{g}}^2, m_{\tilde{t}_1}^2] + \sin^2\theta_{\tilde{t}}\ B_1[p^2, m_{\tilde{g}}^2, m_{\tilde{t}_2}^2]\right), \tag{3.9}$$

$$\Sigma^{(t)R}_{pSQCD}(p^2) = -\frac{C_F}{8\pi^2}g_s^2\left(\sin^2\theta_{\tilde{t}}\ B_1[p^2, m_{\tilde{g}}^2, m_{\tilde{t}_1}^2] + \cos^2\theta_{\tilde{t}}\ B_1[p^2, m_{\tilde{g}}^2, m_{\tilde{t}_2}^2]\right), \tag{3.10}$$

$$\Sigma^{(t)S}_{pSQCD}(p^2) = -\frac{C_F}{8\pi^2}g_s^2 m_{\tilde{g}}\left(\sin\theta_{\tilde{t}}\ \cos\theta_{\tilde{t}}\ e^{-2i\phi}\right)\left(B_0[p^2, m_{\tilde{g}}^2, m_{\tilde{t}_1}^2] - B_0[p^2, m_{\tilde{g}}^2, m_{\tilde{t}_2}^2]\right), \tag{3.11}$$

$$\Sigma^{(t)S\ \ddagger}_{pSQCD}(p^2) = -\frac{C_F}{8\pi^2}g_s^2 m_{\tilde{g}}\left(\sin\theta_{\tilde{t}}\ \cos\theta_{\tilde{t}}\ e^{2i\phi}\right)\left(B_0[p^2, m_{\tilde{g}}^2, m_{\tilde{t}_1}^2] - B_0[p^2, m_{\tilde{g}}^2, m_{\tilde{t}_2}^2]\right), \tag{3.12}$$

Since we don't need the longitudinal part of gluon self-energy in the following calculation, we give the explicit expression for $\Sigma^{(g)T}_{pSQCD}(p^2)$ only.

$$\begin{aligned}\Sigma^{(g)T}_{pSQCD}(p^2) &= \frac{g_s^2}{16\pi^2}\left\{3D\left[(2-D)B_{00}+m_{\tilde{g}}^2B_0-p^2(B_{11}+B_1)\right][p^2,m_{\tilde{g}}^2,m_{\tilde{g}}^2]\right.\\ &+ \left.\sum_{i=1}^{2}\sum_{q=u,d,c}^{s,t,b}\left(A_0[m_{\tilde{q}_i}^2]-2B_{00}[p^2,m_{\tilde{q}_i}^2,m_{\tilde{q}_i}^2]\right)\right\},\end{aligned} \tag{3.13}$$

where $D=4-2\epsilon$ and the definitions of the two-point integrals are adopted from Ref.[23]. In the $SU(3)$ group, $C_F=(N_c^2-1)/(2N_c)$. By using the relevant on-mass-shell renormalization conditions and imposing the real condition on the right-handed top-quark field renormalization constant, $\delta Z_R^t=\delta Z_R^{t\dagger}$[29], we obtain

$$\delta m_t^{pSQCD}=\frac{1}{2}\left(m_t\tilde{Re}\Sigma^{(t)L}_{pSQCD}(m_t^2)+m_t\tilde{Re}\Sigma^{(t)R}_{pSQCD}(m_t^2)+\tilde{Re}\Sigma^{(t)S}_{pSQCD}(m_t^2)+\tilde{Re}\Sigma^{(t)S\ \ddagger}_{pSQCD}(m_t^2)\right), \tag{3.14}$$

$$\begin{aligned}\delta Z_L^{t,pSQCD} &= -\Sigma^{(t)L}_{pSQCD}(m_t^2)-\frac{1}{m_t}\left[\tilde{Re}\Sigma^{(t)S\ \ddagger}_{pSQCD}(m_t^2)-\tilde{Re}\Sigma^{(t)S}_{pSQCD}(m_t^2)\right]\\ &- m_t\frac{\partial}{\partial p^2}\left[m_t\tilde{Re}\Sigma^{(t)L}_{pSQCD}(p^2)+m_t\tilde{Re}\Sigma^{(t)R}_{pSQCD}(p^2)\right.\\ &+ \left.\tilde{Re}\Sigma^{(t)S}_{pSQCD}(p^2)+\tilde{Re}\Sigma^{(t)S\ \ddagger}_{pSQCD}(p^2)\right]|_{p^2=m_t^2},\end{aligned} \tag{3.15}$$

$$\begin{aligned}\delta Z_R^{t,pSQCD} &= -\Sigma^{(t)R}_{pSQCD}(m_t^2)-m_t\frac{\partial}{\partial p^2}\tilde{Re}\left[m_t\Sigma^{(t)L}_{pSQCD}(p^2)+m_t\Sigma^{(t)R}_{pSQCD}(p^2)\right.\\ &+ \left.\Sigma^{(t)S}_{pSQCD}(p^2)+\Sigma^{(t)S\ \ddagger}_{pSQCD}(p^2)\right]|_{p^2=m_t^2},\end{aligned} \tag{3.16}$$

$$\delta Z_g^{pSQCD}=-\tilde{Re}\frac{\partial\Sigma^{(g)T}_{pSQCD}(p^2)}{\partial p^2}|_{p^2=0}, \tag{3.17}$$

where $\tilde{Re}$ only takes the real part of the loop integral functions appearing in the self-energies. The renormalized amplitudes of all the NLO QCD virtual corrections to the partonic processes $q\bar{q}\to t\bar{t}Z^0$ and $gg\to t\bar{t}Z^0$ in the MSSM are expressed as

$$\Delta\mathcal{M}^{ij}_{vir}=\Delta\mathcal{M}^{ij}_{self}+\Delta\mathcal{M}^{ij}_{tri}+\Delta\mathcal{M}^{ij}_{box}+\Delta\mathcal{M}^{ij}_{pent}+\Delta\mathcal{M}^{ij}_{count},\quad (ij=u\bar{u},d\bar{d},gg), \tag{3.18}$$

where $\Delta\mathcal{M}^{ij}_{self}$, $\Delta\mathcal{M}^{ij}_{tri}$, $\Delta\mathcal{M}^{ij}_{box}$, $\Delta\mathcal{M}^{ij}_{pent}$ and $\Delta\mathcal{M}^{ij}_{count}$ represent the amplitudes for self-energy, triangle, box, pentagon and counterterm diagrams, respectively. Then we can get the UV-finite virtual NLO QCD correction component $\Delta\hat{\sigma}^{ij}_{vir}$ as

$$\Delta\hat{\sigma}^{ij}_{vir} = \frac{1}{2|\vec{p}_1|\sqrt{\hat{s}}}\int \mathrm{d}\Gamma_3 \overline{\sum}\mathrm{Re}(\mathcal{M}^{ij}_{LO} \times \Delta\mathcal{M}^{ij}_{vir}). \tag{3.19}$$

The definitions of the notations appeared in above equation are the same with those in Eq.(3.1).

(2) Real gluon and light-(anti)quark emission corrections

In the MSSM, the real $\mathcal{O}(\alpha_s)$ correction processes involve the real gluon emission and real light-(anti)quark emission processes which are listed as follows:

$$q(p_1) + \bar{q}(p_2) \to t(p_3) + \bar{t}(p_4) + Z^0(p_5) + g(p_6) \tag{3.20}$$

$$g(p_1) + g(p_2) \to t(p_3) + \bar{t}(p_4) + Z^0(p_5) + g(p_6) \tag{3.21}$$

$$q(\bar{q})(p_1) + g(p_2) \to t(p_3) + \bar{t}(p_4) + Z^0(p_5) + q(\bar{q})(p_6). \tag{3.22}$$

Because of the IR singularities involved in these processes, we use the two cutoff phase space slicing method (TCPSS) to perform the integration over the phase space of these real emission processes.[31]. In our calculations, the real gluon emission correction to each of the processes $ij \to t\bar{t}Z^0$, $(ij = u\bar{u}, d\bar{d}, gg)$ contains both soft and collinear IR singularities, which are involved in soft gluon region($E_6 \leq \delta_s\sqrt{\hat{s}}/2$) and hard gluon region($E_6 > \delta_s\sqrt{\hat{s}}/2$) respectively. The hard gluon region is also divided into the hard collinear region (HC) and the hard noncollinear region ($\overline{HC}$) with $\frac{2p_i\cdot p_6}{E_6\sqrt{\hat{s}}} < \delta_c$ and $\frac{2p_i\cdot p_6}{E_6\sqrt{\hat{s}}} \geq \delta_c$ (p_i are the momenta for q and $\bar{q}$). Each of the real light-(anti)quark emission processes contains only collinear IR singularity, and can be dealt with in the hard collinear region(HC) too. In the $\overline{HC}$ region, the real emission corrections, $\Delta\hat{\sigma}^{kl}_{\overline{HC}}$, where $kl = q\bar{q}, gg, qg, \bar{q}g$, $(q = u, d)$, are finite and can be calculated numerically with general Monte Carlo method. After summing the virtual and real gluon/(anti)quark radiation corrections, the remained collinear divergence can be cancelled by that in the NLO PDFs. Then the finite total NLO QCD correction to the $pp \to t\bar{t}Z^0 + X$ process can be obtained.

III..3 Total cross sections for the $pp \to t\bar{t}Z^0 + X$ process

The LO, NLO SQCD corrected hadronic cross sections for $pp \to t\bar{t}Z^0 + X$ in the MSSM can be written as:

$$d\sigma_{LO,SNLO}(pp \to t\bar{t}Z^0 + X) = \sum_{ij=u\bar{u},d\bar{d}}^{c\bar{c},s\bar{s},gg} \frac{1}{1+\delta_{ij}} \int_0^1 dx_1 dx_2 \times [G_i(x_1,\mu_f) G_j(x_2,\mu_f) d\hat{\sigma}^{ij}_{LO,SNLO}(x_1 x_2 \sqrt{s},\mu_r) + (1 \leftrightarrow 2)] \quad (3.23)$$

We adopt the CTEQ6L1 and CTEQ6m PDFs[32] in the LO and NLO calculations respectively, except in the specific case for numerical comparison. The $\hat{\sigma}^{ij}_{LO,SNLO}(x_1 x_2\sqrt{s},\mu_r)$ are the LO, NLO SQCD corrected cross sections with the partonic colliding energy $\sqrt{\hat{s}} = x_1 x_2 \sqrt{s}$ for the partonic processes of $ij \to t\bar{t}Z^0 (ij = gg, q\bar{q})$ in the MSSM. Throughout our evaluation, we equate the factorization and renormalization scales and define $\mu = \mu_f = \mu_r$.

In the MSSM, the NLO SQCD corrected partonic cross sections can be expressed as below:

$$d\hat{\sigma}^{ij}_{SNLO}(x_1 x_2\sqrt{s},\mu) = d\hat{\sigma}^{ij}_{LO}(x_1 x_2\sqrt{s},\mu) + d\Delta\hat{\sigma}^{ij}_{SNLO}(x_1 x_2\sqrt{s},\mu) \quad (3.24)$$

where $ij = gg, q\bar{q}$, $\Delta\hat{\sigma}^{ij}_{SNLO}(x_1,x_2,\mu)$ denotes the total NLO QCD correction in the MSSM to the corresponding LO partonic cross section. In this work we ignore reasonably the NLO QCD corrections to the partonic processes $c\bar{c}, s\bar{s} \to t\bar{t}Z^0$ due to the luminosity suppression, i.e., $\Delta\hat{\sigma}^{c\bar{c},\ s\bar{s}}_{SNLO}(x_1 x_2\sqrt{s},\mu) = 0$. Then the full NLO QCD corrections in the MSSM to the process $pp \to t\bar{t}Z^0 + X$ at the LHC can be divided as:

$$\Delta\sigma_{SNLO} = \Delta\sigma_{SM-like} + \Delta\sigma_{pSQCD}. \quad (3.25)$$

The later part arises from the virtual correction of the diagrams with gluino/squark in loops. Note that the cross sections for the parent process $pp \to t\bar{t}Z^0 + X$ $\sigma_{SM-like}$ should be the same as the corresponding ones, σ_{SM}, in the SM[19, 33].

IV. Numerical Results and discussions

In this section, we present numerical results of the NLO QCD corrections to the process $pp \to t\bar{t}Z^0 + X$ in the MSSM at the LHC. The numerical results for the LO and the NLO SM-like QCD

μ	our σ_{LO}(pb)	our σ_{NLO}(pb)	σ_{LO}(pb) in Ref.[33]	σ_{NLO}(pb) in Ref.[33]
$\mu_0/4$	1.0779(8)	1.216(5)	1.078	1.213
$\mu_0/2$	0.8083(6)	1.095(4)	0.808	1.093
μ_0	0.6198(3)	0.975(4)	0.620	0.973

Table 1: The comparison of our numerical results for the $pp \to t\bar{t}Z^0 + X$ process in the SM at the LHC with those in Ref.[33], where the LO and NLO QCD corrected cross sections for different energy scale values($\mu = \mu_f = \mu_r$) are listed with the relevant parameters and the PDFs being the same as in Ref.[33], i.e., $\mu_0 = 2m_t + m_Z$, $m_t = 170.9\ GeV$, $m_Z = 91.19\ GeV$, $m_W = 80.45\ GeV$ and the MRST PDFs. Note that the numerical results are contributed by the subprocesses $q\bar{q}, gg \to t\bar{t}Z^0$ with $q = u, d, c, s$ at the LO, but $q = u, d$ at the NLO.

corrections have been compared with the data presented in Tabel 1 of Ref.[33]. Both result sets are listed in Table 1. There we employ the MRST PDFs[34] and the input parameters which were used in Ref.[33]. The agreement between them can be seen obviously from the table.

In the following numerical calculations in the frameworks of the SM and MSSM, we define $\mu_0 \equiv m_t + m_Z/2$ and take CTEQ6L1 PDFs with an one-loop running α_s in the LO calculation and CTEQ6M PDFs with a two-loop α_s in the NLO calculation[35]. The number of active flavors is $N_f = 5$ and the QCD parameters are $\Lambda_5^{LO} = 166\ MeV$ and $\Lambda_5^{\overline{MS}} = 227\ MeV$ for the LO and NLO calculations, respectively[35]. We ignore the masses of u-, d-, and s-quarks in our calculations. The other SM parameters are taken as[35],

$$\alpha_{ew}({m_Z}^2) = 1/127.918, \quad m_t = 171.2\ GeV, \quad m_b = 4.2\ GeV, \quad m_c = 1.3\ GeV,$$
$$m_Z = 91.1876\ GeV, \quad m_W = 80.398\ GeV, \quad \sin^2\theta_W = 1 - m_W^2/m_Z^2 = 0.222646. \tag{4.1}$$

For the SUSY parameters of the scalar top sector in the CP-conserving MSSM, we take the top squark masses($m_{\tilde{t}_1}$, $m_{\tilde{t}_2}$) and their mixing angle(θ_t) as input parameters, and adopt Eq.(2.9) to calculate the $m_{\tilde{t}_L}^2$, $m_{\tilde{t}_R}^2$, a_t, and sequentially use Eq.(2.3) to get the SUSY soft-breaking parameters $\tilde{M}_{Q_t}$ and $\tilde{M}_{U_t}$ for the stop sector by assuming $\tan\beta = 10$(Here we take $\tan\beta = 10$ arbitrarily, because the NLO SQCD cross sections for $pp \to t\bar{t}Z^0 + X$ do not directly related to $\tan\beta$, and in the range of $1 < \tan\beta < 50$ the dependences of $m_{\tilde{t}_1}$ and $m_{\tilde{t}_2}$ on $\tan\beta$ are rather weak[11]). Since the gauge invariance in the MSSM requires $\tilde{M}_{Q_b} = \tilde{M}_{Q_t}$, we need only to fix two additional parameters for the scalar bottom sector. We neglect the mixing for

the scalar bottom sector and assume $m_{\tilde{b}_L} = m_{\tilde{b}_R}$, the masses of $\tilde{b}_{1,2}$ can be obtained by the following equation,

$$m^2_{\tilde{b}_L} = \tilde{M}^2_{Q_t} + m^2_b + m^2_Z(I^3_b - Q_b s^2_W)\cos 2\beta. \tag{4.2}$$

Furthermore, we take $m_{\tilde{g}} = 200\ GeV$[36], $\phi_q = 0$ (for the u-, d-, c-, s-, b-quarks) and let CP-phase $\phi \equiv \phi_t \neq 0$ as a free parameter in the CP-violating MSSM. For the first two squark generations, we take the assumption of the universal squark mass as used in Ref.[11] i.e.,

$$m_{\tilde{u}_L} = m_{\tilde{u}_R} = m_{\tilde{d}_L} = m_{\tilde{d}_R} = m_{\tilde{c}_L} = m_{\tilde{c}_R} = m_{\tilde{s}_L} = m_{\tilde{s}_R} = m_{\tilde{q}}, \tag{4.3}$$

and set $m_{\tilde{q}} = 1\ TeV$ in the following calculations.

To make the demonstration of the correctness of our calculation for the integrations over the phase space of the 4-body final-state real emission processes, we have checked the independence of the SM-like NLO QCD correction component $\Delta\sigma^{SM-like}_{SNLO}$ of the process $pp \to u\bar{u} \to t\bar{t}Z^0 + X$ on the two cutoffs δ_s and δ_c separately shown in Figs.7(a-b) and Figs.8(a-b) separately. In identifying the $\Delta\sigma^{SM-like}_{SNLO}$ independence on δ_s, we fix $\delta_c = 1 \times 10^{-6}$ and vary δ_s from 4×10^{-4} to 8×10^{-3}. For probing the $\Delta\sigma^{SM-like}_{SNLO}$ independence on δ_c, we take $\delta_s = 1 \times 10^{-3}$ and let δ_c running from 1×10^{-6} to 4×10^{-5}. These four figures show that although the three-body correction($\Delta\sigma^{(3)}$) and four-body correction($\Delta\sigma^{(4)}$) are strongly related to the cutoffs δ_s and δ_c, the final total SM-like NLO QCD correction $\Delta\sigma^{SM-like}_{SNLO}$ to the $pp \to u\bar{u} \to t\bar{t}Z^0 + X$ process, which is the summation of the three-body term and four-body term, i.e., $\Delta\sigma^{SM-like}_{SNLO} = \Delta\sigma^{(3)} + \Delta\sigma^{(4)}$, is indeed independent of the cutoffs (δ_s and δ_c) within the statistical errors.

The LO and NLO QCD corrected cross sections in the CP-conserving MSSM for the process $pp \to t\bar{t}Z^0 + X$ as the functions of the renormalization and fatorization scales in the $\mu \equiv \mu_r = \mu_f$ way at the LHC, are demonstrated in Fig.9(a). The curve for the component of the SM-like NLO QCD corrected cross section is also shown there for the comparison. The corresponding K-factors for the NLO SQCD and SM-like QCD corrections, which are defined as $K(\mu) \equiv \sigma_{SNLO}(\mu)/\sigma_{LO}(\mu)$ and $K_{SM-like}(\mu) \equiv \sigma^{SM-like}_{SNLO}(\mu)/\sigma_{LO}(\mu)$, are drawn in Fig.9(b), respectively. There we take $\mu_0 = m_t + m_Z/2$, $m_{\tilde{g}} = 200GeV$ and μ running from $\mu_0/5$ to $3\mu_0$. As we know, the scale dependence of the PDFs for the incoming u- and d-quarks are significant,

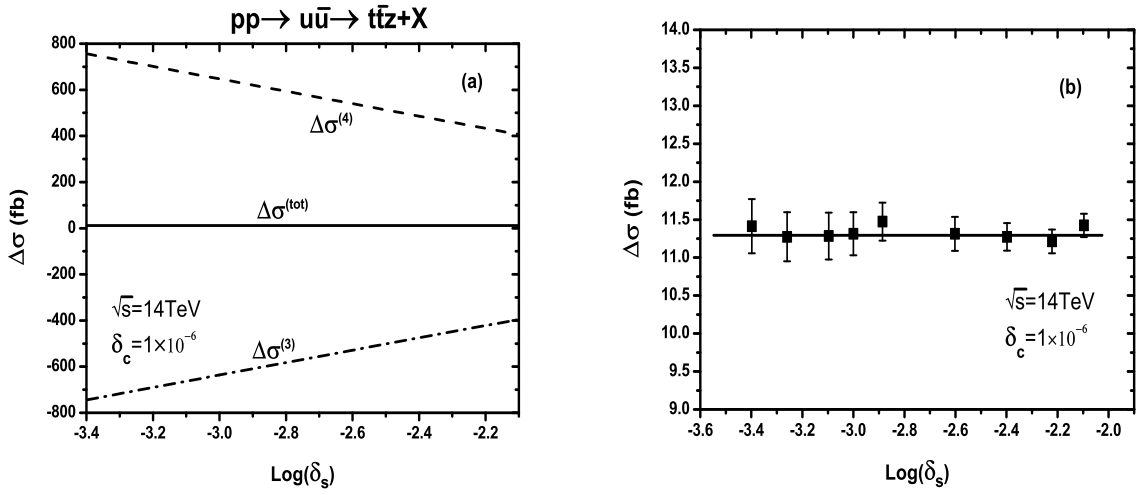

Figure 7: (a) The dependence of QCD NLO correction parts to the $pp \to u\bar{u} \to t\bar{t}Z^0 + X$ process on the soft cutoff δ_s at the LHC with the collinear cutoff $\delta_c = 1\times10^{-6}$ and $\sqrt{s} = 14\,TeV$. (b) The amplified curve for the total QCD correction $\Delta\sigma^{SM-like}_{SNLO}$ to the process $pp \to u\bar{u} \to t\bar{t}Z^0 + X$, where it includes the calculation errors.

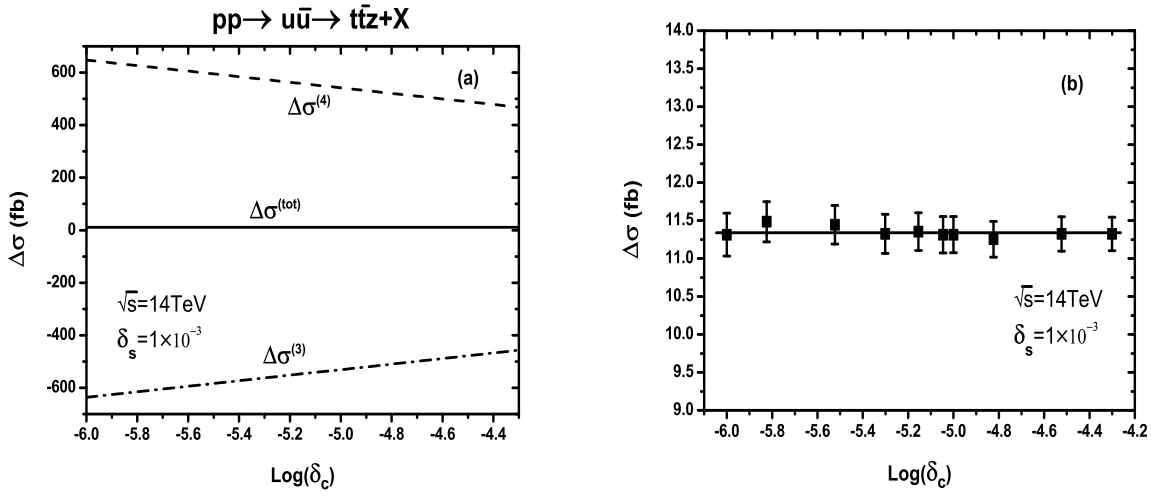

Figure 8: (a) The dependence of the QCD NLO correction parts to the $pp \to u\bar{u} \to t\bar{t}Z^0 + X$ process on the collinear cutoff δ_c at the LHC with $\delta_s = 1\times10^{-3}$ and $\sqrt{s} = 14\,TeV$. (b) The amplified curve for the total QCD correction $\Delta\sigma^{SM-like}_{SNLO}$ to the process $pp \to u\bar{u} \to t\bar{t}Z^0 + X$, where it includes the calculation errors.

even up to the NLO the scale dependence of the results are not too small. Since the $t\bar{t}Z^0$ production at the LHC is a QCD process at the LO, the scale dependence of the NLO SM-like QCD corrected cross section (dotted curve in Fig.9(a)) is less than that of the LO cross section for the $pp \to t\bar{t}Z^0 + X$ process. On the other hand, the pSQCD correction is to some extend a LO contribution, because this process does not involve the supersymmetric strong coupling $\hat{g}_s$ at the LO. Therefore, the pSQCD correction induces some more scale dependence to the $pp \to t\bar{t}Z^0 + X$ process. Considering the fact that pSQCD correction is quite small comparing with the SM-like QCD correction demonstrated in Fig.9(a), the scale dependence of the full SQCD corrected cross section is similar to that of the SM-like QCD corrected cross section, which is much less than that of the LO cross section. Actually, Fig.9(a) demonstrates that the LO cross section is strongly correlated with the energy scale μ, while the NLO QCD corrections obviously improve the scale uncertainties in both the CP-conserving MSSM and the SM. Comparing with the SM-like NLO QCD correction, it can be seen the pSQCD corrections cancellate the correction part from the SM-like QCD, and the NLO pSQCD correction to the total cross section can exceed -4.75% in our chosen parameters space. Fig.9(a) shows that the total NLO SQCD K-factor changes from 0.48 to 1.63 as the scale μ running from $\mu_0/5$ to $3\mu_0$. In the following calculations we set $\mu = \mu_0$.

Fig.10(a) shows the LO and NLO QCD corrected cross sections in the CP-conserving MSSM and the SM for the process $pp \to t\bar{t}Z^0 + X$ as the functions of the gluino mass ($m_{\tilde{g}}$) at the LHC by taking $m_{\tilde{t}_1} = 100GeV$, $m_{\tilde{t}_2} = 600GeV$, and the mixing angle $\theta_t = -\pi/4$ for the stop sector. The corresponding K-factors for the NLO SQCD and SM-like QCD corrections versus $m_{\tilde{g}}$ are depicted in Fig.10(b), respectively. Figs.10(a) and 10(b) demonstrate that although the SM-like curves have no relation with gluon mass, the curves for NLO SQCD corrections is clearly related with $m_{\tilde{g}}$ in the region of $m_{\tilde{g}} < 300\ GeV$. The NLO SQCD corrected cross section (and K-factors) approaches a constant when $m_{\tilde{g}} > 400\ GeV$ due to the decoupling effect for heavy gluino exchanging. We can see that the NLO pSQCD correction is non-zero when $m_{\tilde{g}} > 400\ GeV$, because of the relatively light mass of $\tilde{t}_1$ in loops ($m_{\tilde{t}_1} = 100\ GeV$). Fig.10(b) shows when we take $m_{\tilde{g}} = 100\ GeV$, the pSQCD relative correction can reach to -8.56% and

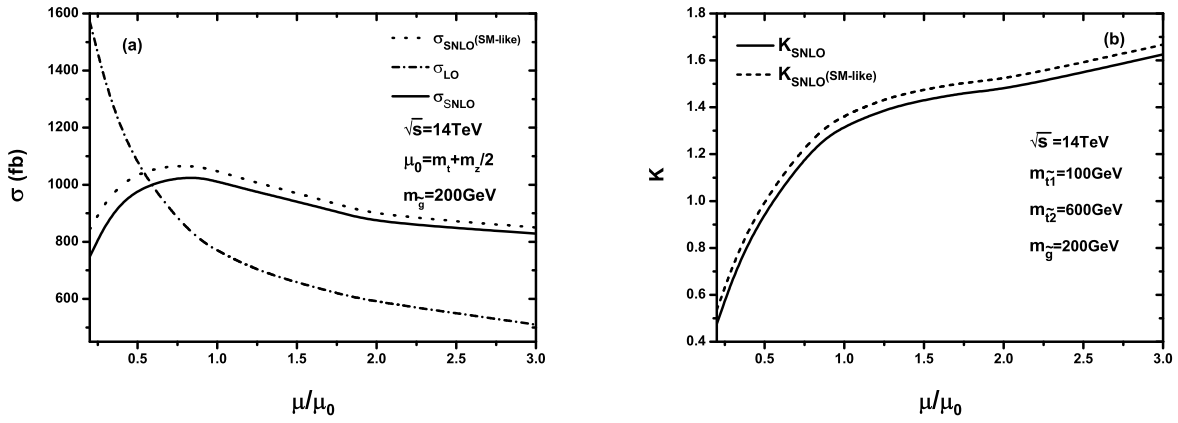

Figure 9: (a) The dependence of the LO and NLO cross sections in the CP-conserving MSSM and the SM on the energy scale at the LHC. (b) The total NLO QCD K-factors for the process($K_{SNLO}(\mu) \equiv \sigma_{SNLO}(\mu)/\sigma_{LO}(\mu)$) and the NLO QCD K-factors of the SM-like part ($K_{SM-like}(\mu) = \sigma_{SNLO}^{SM-like}(\mu)/\sigma_{LO}(\mu)$) for the $pp \to t\bar{t}Z^0 + X$ process versus the energy scale at the LHC.

K-factor of the total SQCD correction will be 1.281, while when we fix $m_{\tilde{g}} = 200\ GeV$, we get -4.75% for the corresponding pSQCD relative correction and 1.319 for the K-factor of the SQCD correction.

We present Fig.11(a) to show the relations between the LO and NLO QCD corrected cross sections in the CP-conserving MSSM and SM for the process $pp \to t\bar{t}Z^0 + X$ at the LHC as the functions of $m_{\tilde{t}_1}$, one of the input parameters for stop sector. Here we take $m_{\tilde{g}} = 200\ GeV$, the other two input parameters for stop sector are set as $m_{\tilde{t}_2} = 600GeV$, $\theta_t = -\pi/4$, and the other SUSY parameters are obtained as explained above. The corresponding K-factors for the NLO SQCD and SM-like NLO QCD corrections versus $m_{\tilde{t}_1}$ are depicted in Fig.11(b), respectively. Again we see from Figs.11(a) and (b) that the SM-like curves do not show the dependence on $m_{\tilde{t}_1}$, but the NLO QCD corrections in the MSSM obviously rely on $m_{\tilde{t}_1}$ in the region of $m_{\tilde{t}_1} < 400\ GeV$. While in the region of $m_{\tilde{t}_1} > 400\ GeV$ the NLO QCD corrections and corresponding K-factors in the MSSM tend to be constant respectively, because there exists the decoupling effect of heavy $\tilde{t}_1$ in loops, and the nonzero NLO pSQCD correction is induced by the relatively light mass of gluon in loops($m_{\tilde{g}} = 200\ GeV$). From Fig.11(b) we can see that with the mass of $\tilde{t}_1$ running from 100 GeV to 500 GeV, the NLO pSQCD relative correction

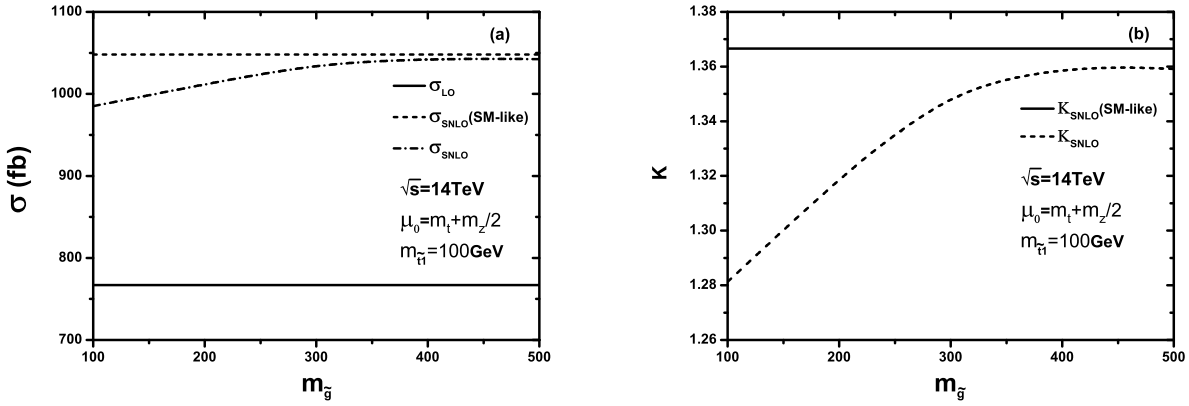

Figure 10: (a) The LO and NLO QCD corrected cross sections in the CP-conserving MSSM as the functions of the gluino mass $m_{\tilde{g}}$ at the LHC. (b) The corresponding total NLO QCD K-factor in the MSSM for the process $pp \to t\bar{t}Z^0 + X$ ($K_{SNLO}(m_{\tilde{g}}) \equiv \frac{d\sigma_{SNLO}}{dm_{\tilde{g}}}/\frac{d\sigma_{LO}}{dm_{\tilde{g}}}$) and the NLO QCD K-factor for the SM-like part for the $pp \to t\bar{t}Z^0 + X$ process versus the gluino mass at the LHC.

varies from -4.75% to -0.25%, and the K-factor of the total NLO SQCD changes from 1.319 to 1.364.

The LO and NLO QCD corrected differential cross sections of the transverse momenta for top quark and Z^0 boson in the CP-conserving MSSM and the SM for the process $pp \to t\bar{t}Z^0 + X$ at the LHC, are drawn in Fig.12(a) and Fig.13(a), separately. In these plots we take $m_{\tilde{t}_1} = 100GeV$, $m_{\tilde{t}_2} = 600GeV$ and the mixing angle $\theta_t = -\pi/4$ for stop sector, $m_{\tilde{g}} = 200\ GeV$, and the other SUSY parameters are set to have the values explained above. Their corresponding K-factors($K(p_T) \equiv \frac{d\sigma_{SNLO}}{dp_T}/\frac{d\sigma_{LO}}{dp_T}$) are depicted in Figs.12(b) and Fig.13(b), respectively. There we take $m_{\tilde{g}} = 200\ GeV$. Both figures Fig.12(a) and Fig.13(a) show that the SM-like NLO QCD corrections enhance the differential cross sections of the transverse momenta for the top quark and Z^0 boson in whole plotted range, while the NLO pSQCD correction part suppresses the SM-like QCD correction slightly. We can obtain from Fig.12(b) and Fig.13(b) that the relative corrections from the pSQCD can be -8.56% and -8.12% when $p_T^t \sim 105\ GeV$ and $p_T^Z \sim 135\ GeV$ respectively. And in these two figures there exist obvious distortions for the two NLO SQCD K-factor curves compared with the corresponding SM-like ones. Those curve distortions are caused by the resonant effect of gluon self-energy.

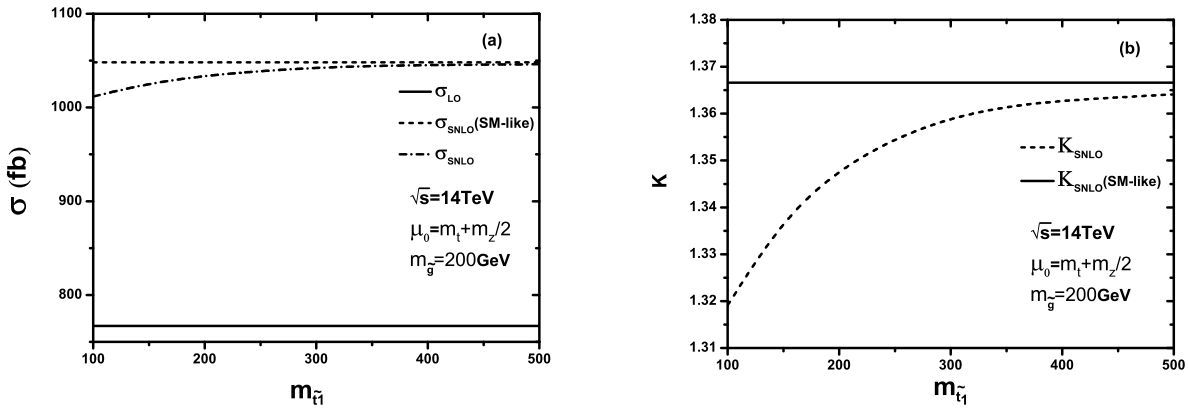

Figure 11: (a) The LO and NLO QCD corrected cross sections in the CP-conserving MSSM as the functions of the light scalar top-quark mass $m_{\tilde{t}_1}$ at the LHC. (b) The corresponding total NLO QCD K-factor in the MSSM for the process $pp \to t\bar{t}Z^0 + X$ ($K(m_{\tilde{t}_1}) \equiv \frac{d\sigma_{SNLO}}{dm_{\tilde{t}_1}} / \frac{d\sigma_{LO}}{dm_{\tilde{t}_1}}$) and the NLO QCD K-factor for the SM-like part for the $pp \to t\bar{t}Z^0 + X$ process versus $m_{\tilde{t}_1}$ at the LHC.

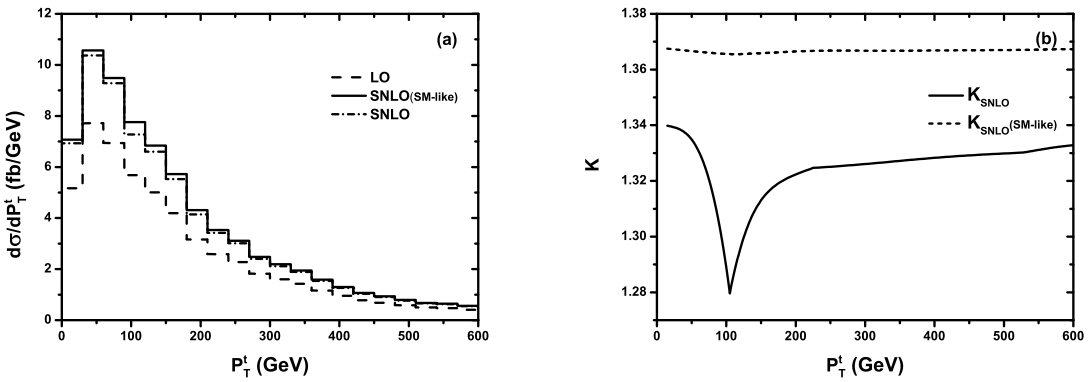

Figure 12: The LO and NLO QCD corrected distributions of the transverse momentum of the top quark for the process $pp \to t\bar{t}Z^0 + X$ in the SM and CP-conserving MSSM at the LHC and the corresponding K-factors($K(p_T^t) \equiv \frac{d\sigma_{SNLO}}{dp_T^t} / \frac{d\sigma_{LO}}{dp_T^t}$) versus p_T^t. (a) the differential cross section of the transverse momentum, (b) the corresponding K-factors.

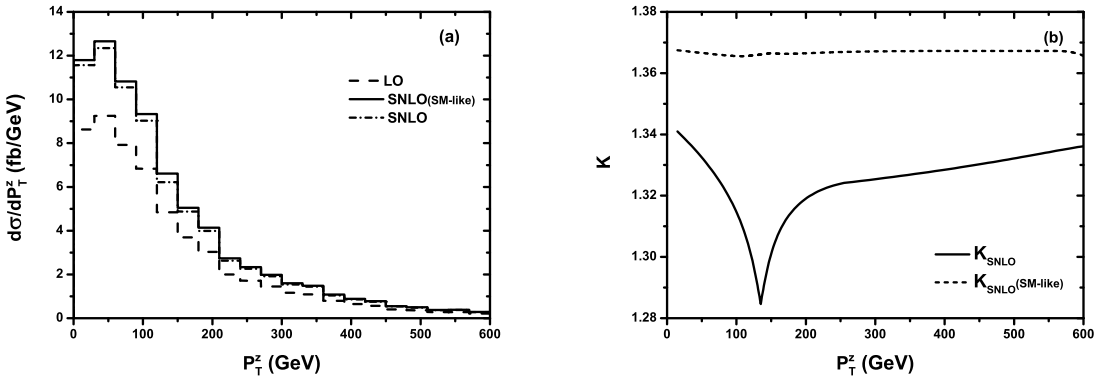

Figure 13: The LO and NLO QCD corrected distributions of the transverse momentum of the Z^0-boson for the process $pp \to t\bar{t}Z^0 + X$ in the SM and CP-conserving MSSM at the LHC and the corresponding K-factors($K(p_T^Z) \equiv \frac{d\sigma_{SNLO}}{dp_T^Z} / \frac{d\sigma_{LO}}{dp_T^Z}$) versus p_T^Z. (a) the differential cross section of the transverse momentum, (b) the corresponding K-factors.

In Fig.14, we define $K(M_{(t\bar{t})}) = \frac{d\sigma_{SNLO}}{dM_{(t\bar{t})}} / \frac{d\sigma_{LO}}{dM_{(t\bar{t})}}$ and plot the curves for the differential cross sections and corresponding K-factor as the functions of the top-pair invariant mass $M_{(t\bar{t})}$, where we take $m_{\tilde{t}_1} = 100GeV$, $m_{\tilde{t}_2} = 600GeV$, $\theta_t = -\pi/4$ for stop sector, and $m_{\tilde{g}} = 200\ GeV$. There we see the $K(M_{(t\bar{t})})$ distribution demonstrates the characteristic effects, which are shown already on the K-factor curves in Fig.12(b) and Fig.13(b). The distortion of the K-factor distribution curve for $M_{(t\bar{t})}$ is located at the vicinity of $M_{(t\bar{t})} \sim 2m_{\tilde{g}} = 400\ GeV$ where the K-factor of the NLO SQCD correction reaches the value of 1.457. It exhibits exactly that the resonance effect of the gluino-pair threshold in the gluon self-energy induces the curve distortion.

If the CP-violating MSSM is true, the CP-odd effects for the process $pp \to t\bar{t}Z^0 + X$ at the LHC would be demonstrated through the cross section deviation from the CP-conserving MSSM, and shown from a nonzero CP-odd observable $\mathcal{A}_\Phi$ defined in Eq.(2.17). We plot the NLO SQCD corrections to the cross sections of $pp \to t\bar{t}Z^0 + X$ process as the functions of the CP-phase ϕ in Fig.15(a), and the corresponding K-factors are drawn in Fig.15(b). In these two figures we set $\phi \equiv \phi_t$ and $\phi_q = 0$, $(q = u, d, s, c, b)$, $m_{\tilde{g}} = 200\ GeV$, for the stop sector we take two set of input parameters: (1) $\{m_{\tilde{t}_1}, m_{\tilde{t}_2}, \theta_t\} = \{100GeV, 600GeV, -\frac{\pi}{4}\}$(dash-dotted-curve); (2) $\{m_{\tilde{t}_1}, m_{\tilde{t}_2}, \theta_t\} = \{250GeV, 800GeV, -\frac{\pi}{4}\}$(dotted-curve), and the other SUSY parameter values are explained above. The curve for the SM-like NLO QCD correction(full-

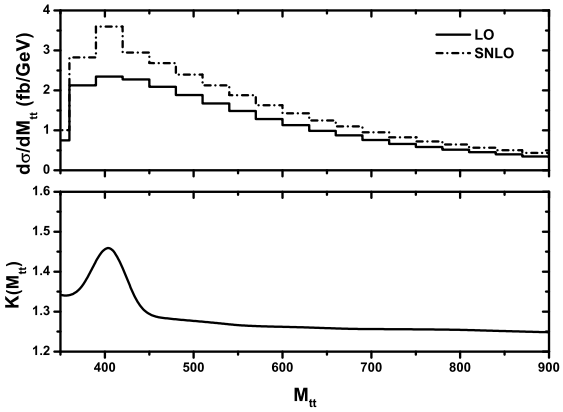

Figure 14: The LO and NLO QCD corrected differential cross sections of the top-pair invariant mass $M_{(t\bar{t})}$ and the corresponding K-factors in the CP-conserving MSSM at the LHC.

line) in Fig.15(a) shows the SM-like correction part does not depend on the CP-phase, while the curves for NLO SQCD correction part vary as cosine wave of ϕ. The curves for K-factors of the SM-like QCD and the SQCD correction in Fig.15(b), show the similar behaviors with the corresponding ones in Fig.15(a).

We adopt the CP-asymmetry parameter($\mathcal{A}_\Phi$) definition in Eq.(2.17) and depict $\mathcal{A}_\Phi$ as the function of CP-phase ϕ in Fig.16, where $m_{\tilde{g}} = 200\ GeV$ and the solid curve is for taking $\{m_{\tilde{t}_1}, m_{\tilde{t}_2}, \theta_t\} = \{100GeV, 600GeV, -\frac{\pi}{4}\}$, the dash-dotted curve $\{m_{\tilde{t}_1}, m_{\tilde{t}_2}, \theta_t\} = \{250GeV, 800GeV, -\frac{\pi}{4}\}$. It shows that the two curves for $\mathcal{A}_\Phi$ are sinusoidal with respect to Φ, and the absolute value of $\mathcal{A}_\Phi$ for $\{m_{\tilde{t}_1}, m_{\tilde{t}_2}, \theta_t\} = \{100GeV, 600GeV, -\frac{\pi}{4}\}$ can reach its maximum of 2.17×10^{-3} when $\phi = \frac{n\pi}{4}, (n = 1, 3, 5, 7)$, while it can be 1.57×10^{-3} for $\{m_{\tilde{t}_1}, m_{\tilde{t}_2}, \theta_t\} = \{250GeV, 800GeV, -\frac{\pi}{4}\}$. From Eq.(2.19) we can see that if we assume the total cross section of the process $pp \to t\bar{t}Z^0 + X$ is 1 pb and the integral luminosities are larger than 212 fb^{-1}, 1911 fb^{-1} or 5309 fb^{-1} we may observe the CP-violating effect induced by ϕ at 1σ, 3σ or 5σ significance for the case of $\{m_{\tilde{t}_1}, m_{\tilde{t}_2}, \theta_t\} = \{100GeV, 600GeV, -\frac{\pi}{4}\}$, and 406 fb^{-1}, 3651 fb^{-1} or 10142 fb^{-1} for the case of $\{m_{\tilde{t}_1}, m_{\tilde{t}_2}, \theta_t\} = \{250GeV,\ 800GeV, -\frac{\pi}{4}\}$, respectively.

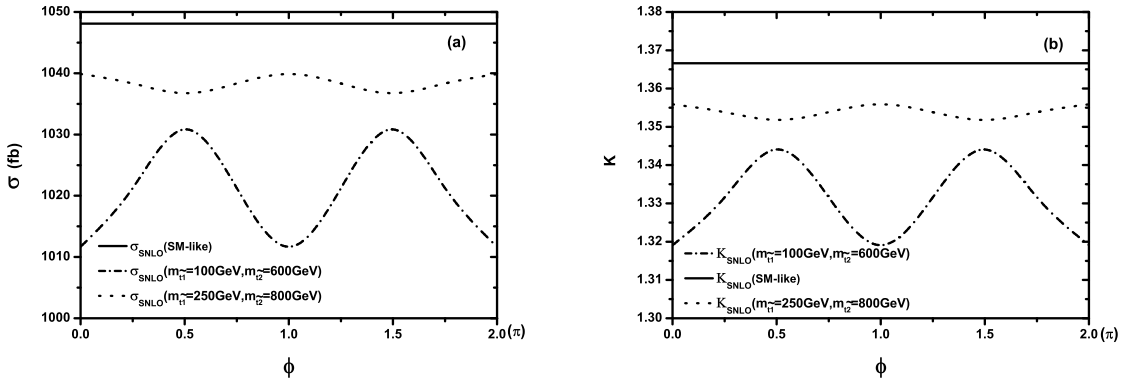

Figure 15: (a) The LO and NLO QCD corrected cross sections as the functions of the CP-phase $\phi(\equiv \phi_t)$ for the process $pp \to t\bar{t}Z^0 + X$ at the LHC. (b) The corresponding total NLO QCD K-factors versus CP phase ϕ.

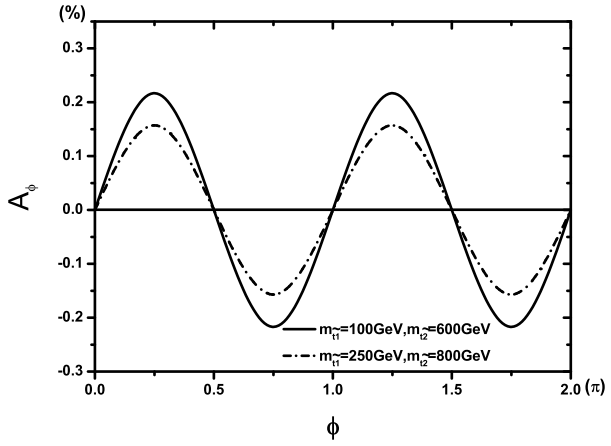

Figure 16: The CP-violating asymmetry parameter $\mathcal{A}_\Phi$ as the functions of the CP-phase angle ϕ for the process $pp \to t\bar{t}Z^0 + X$ at the LHC, where the solid curve is for $\{m_{\tilde{t}_1}, m_{\tilde{t}_2}, \theta_t\} = \{100GeV, 600GeV, -\pi/4\}$, and the dashed curve for $\{m_{\tilde{t}_1}, m_{\tilde{t}_2}, \theta_t\} = \{250GeV, 800GeV, -\pi/4\}$.

V. Conclusion

In this paper, we study the total NLO QCD corrections for the process $pp \to t\bar{t}Z^0 + X$ in the MSSM at the LHC. Our results show that both the total NLO QCD corrections in the CP-conserving MSSM and the SM improve the LO scale uncertainty. We provide the NLO QCD corrected distributions of transverse momenta of the top-quark and Z^0 boson at the LHC in the CP-conserving MSSM and the SM. There we can see that the total NLO QCD corrections can modify significantly the LO cross sections respectively. The pSQCD corrections to the process $pp \to t\bar{t}Z^0 + X$ can be beyond -8% when we take $m_{\tilde{g}} = 200\ GeV$ and restrict the top-quark $90GeV < p_T^t < 120\ GeV$ or the Z^0 boson $120\ GeV < p_T^Z < 150\ GeV$. And we see that the K-factor is sensitive to the value of $m_{\tilde{g}}$ or $m_{\tilde{t}_1}$ in the relatively lighter mass region of $\tilde{g}$ or $\tilde{t}_1$. Furthermore, we find that if the CP-violating phase really exists in the scalar top mixing matrix or in the Majorana mass term of the gluino predicted by the CP-violating MSSM, the CP-violating effect, described by CP-violating asymmetry parameter $\mathcal{A}_\Phi$, can be expected to be the order of 10^{-3} and reach the maximal value 2.17×10^{-3}. Therefore, testing CP-violation induced by CP-phase ϕ in $pp \to t\bar{t}Z^0 + X$ process could be an interesting task at the LHC.

Acknowledgments: This work was supported in part by the National Natural Science Foundation of China(No.10875112, No.10675110), the Specialized Research Fund for the Doctoral Program of Higher Education(No.20093402110030), and the China Postdoctoral Science Foundation(No.20080440103).

References

[1] S. L. Glashow, Nucl. Phys. **22** (1961) 579; S. Weinberg, Phys. Rev. Lett. **19** (1967) 1264; A. Salam, Proc. 8th Nobel Symposium Stockholm 1968,ed. N. Svartholm (Almquist and Wiksells, Stockholm 1968) p.367; H. D. Politzer, Phys. Rep. **14** (1974) 129.

[2] P. W. Higgs, Phys. Lett **12** (1964) 132, Phys. Rev. Lett. **13** (1964) 508; Phys. Rev. **145** (1966) 1156; F. Englert and R.Brout, Phys. Rev. Lett. **13** (1964) 321; G. S. Guralnik, C.

R. Hagen and T. W. B. Kibble, Phys. Rev. Lett. **13** (1964) 585; T. W. B. Kibble, Phys. Rev. **155** (1967) 1554.

[3] P. Fayet, and S. Ferrara Phys. Rept. **32**, 249(1977).

[4] H.P. Nilles, Phys. Rept. **110**, 1(1984).

[5] H.E. Haber and G.L. Kane, Phys. Rept. **117**, 75(1985).

[6] J. Wess and J. Bagger,'Supersymmetry and supergravity', Princeton, USA: University Press (1992) p259.

[7] W. M. Yao *et al.*, J. Phys. **G33**, 1 (2006).

[8] H.E. Haber and G. Kane, Phys. Rep. 117(1985)75; J.Gunion and H.E. Haber, Nucl. Phys. **B272**, (1986)1.

[9] F. Abe, *et al.* (CDF Collaboration), Phys. Rev. Lett. **74**, 2626 (1995).

[10] S. Abachi, *et al.* (DØ Collaboration), Phys. Rev. Lett. **74**, 2632 (1995).

[11] S. Berge, W. Hollik, W.M. Mosle, and D. Wackeroth, Phys. Rev. **D76**,034016(2007), arXiv: hep-ph/0703016v1.

[12] K. Hagiwara, H. Murayama and I. Watanabe, Nucl. Phys. **B367**(1991), 257.

[13] L. Dai, W.G. Ma, R.Y. Zhang, L. Guo, and S.M. Wang, Phys. Rev. **D78**, 094010 (2008).

[14] S. Bar-Shalom, D. Atwood, and A. Soni, Phys. Lett**B419**(1998) 340.

[15] B. Grzadkowski and J. Pliszka, Phys. Rev. **D60**(1999)115018.

[16] Lali Chatterjee, Cheuk-Yin Wong, arXiv: hep-ph/9501218.

[17] A. Denner, S. Dittmaier, M. Strobel, Phys. Rev. **D53** (1996) 44.

[18] Dong Chuan-Fei, Ma Wen-Gan, Zhang Ren-You, Guo Lei, and Wang Shao-Ming, Commu Theor. Phys. 52(2009)302-310, arXiv:0812.4728v1[hep-ph].

[19] A. Lazopoulos, K. Melnikov, F. Petriello, Phys. Rev. **D77**, 034021(2008), arXiv: 0709.4044v1.

[20] J. Ellis and S. Rudaz, Phys. Lett. **B128**, 248(1983).

[21] T. Han, and Y. Li, MADPH-09-1549, NPAC-09-15, arXiv:0911.2933v1 [hep-ph].

[22] P. Nason, S. Dawson, R.K. Ellis, Nucl. Phys. **B327** (1989) 49; Nucl. Phys. **B335** (1989)260 (E).

[23] A. Denner, Fortschr. Phys. **41**, 307 (1993).

[24] G. Passarino and M. Veltman, Nucl. Phys. **B160**, 151 (1979).

[25] M. Chanowitz, M. Furman, and I. Hinchliffe, Nucl. Phys. **B159**(1979)225.

[26] T. Hahn, Comput. Phys. Commun 140, 418 (2001).

[27] R. Mertig, M. Böhm, A. Denner, Comput. Phys. Commun. **64**(1991)345.

[28] G. J. van Oldenborgh, NIKHEF-H/90-15; T. Hahn, M. Perez-Victoria, Comput. Phys. Commun. **118** (1999)153.

[29] Han Liang, Ma Wen-Gan and Yu Zeng-Hui, Phys. Rev. **D56**(1997)265.

[30] Bernd A. Kniehl and A. Pilaftsis, Nucl. Phys. **B474**(1996)286.

[31] B. W. Harris and J.F. Owens, Phys. Rev. **D65** (2002) 094032.

[32] J. Pumplin *et al.*, JHEP 0207, 012 (2002); D. Stump *et al.*, JHEP 0310, 046 (2003).

[33] A. Lazopoulos, T. McElmurry, K. Melnikov and F. Petriello, Phys. Lett. **B666**,62(2008).

[34] A. D. Martin, R. G. Roberts, W. J. Stirling and R. S. Thorne, Eur. Phys. J. C23, 73 (2002); Phys. Lett. **B531**, 216(2002).

[35] C. Amsler,*et al.* Phys. Lett. **B667**,1 (2008).

[36] V.M. Abazov *et al.*(DØ Collaboration), Phys. Lett. **B638**, 119(2006), arXiv: hep-ex/0604029; V.M. Abazov *et al.*(DØ Collaboration) (2006), arXiv: hep-ex/0611003; A.A. Affolder *et al.*(CDF Collaboration) Phys. Rev. Lett. **88**, 041801(2002), arXiv: hep-ex/0106001; A.A. Affolder *et al.*(CDF Collaboration) Phys. Rev. Lett. **87**, 251803(2001), arXiv: hep-ex/0106061.